

Uniaxial pressure effects in the two-dimensional van der Waals ferromagnet CrI₃

J. Arneth¹, M. Jonak¹, S. Spachmann¹, M. Abdel-Hafiez^{2,3}, Y. O. Kvashnin^{4,*} and R. Klingeler^{1,†}

¹Kirchhoff Institute of Physics, Heidelberg University, INF 227, D-69120 Heidelberg, Germany

²Department of Physics and Astronomy, Uppsala University, Box 516, SE-751 20 Uppsala, Sweden

³National University of Science and Technology "MISIS", Moscow 119049, Russia

⁴Department of Physics and Astronomy, Division of Materials Theory, Uppsala University, Box 516, SE-751 20 Uppsala, Sweden



(Received 19 August 2021; revised 10 January 2022; accepted 3 February 2022; published 14 February 2022)

Magnetoelastic coupling and uniaxial pressure dependencies of the ferromagnetic ordering temperature in the quasi-two-dimensional layered van der Waals material CrI₃ are experimentally studied and quantified by high-resolution dilatometry. Clear anomalies in the thermal expansion coefficients at T_C imply positive (negative) pressure dependencies $\partial T_C / \partial p_i$ for pressure applied along (perpendicular to) the c axis. The experimental results are backed up by numerical studies showing that the dominant, intralayer magnetic coupling increases upon compression along the c direction and decreases with negative in-plane strain. In contrast, interlayer exchange is shown to initially increase and subsequently decrease upon the application of both out-of-plane and in-plane compression.

DOI: [10.1103/PhysRevB.105.L060404](https://doi.org/10.1103/PhysRevB.105.L060404)

Introduction. Quasi-two-dimensional (quasi-2D) layered van der Waals (vdW) materials have been intensively studied in recent years due to their rich physics including long-range-ordered phases down to the single layer [1–4]. Thanks to the layered structure, they allow one to address the fundamentals of low-dimensional physics and also hold an outstanding promise for technological applications, as demonstrated, e.g., by Cr₂Ge₂O₆/NiO heterostructures or NiPS₃-based field-effect transistors [5,6]. In CrI₃, ferromagnetism emerges in the bulk at $T_C = 61$ K, and persists even down to the monolayer thickness with a slightly reduced ordering temperature [1]. As magnetic long-range order in isotropic 2D spin systems is supposed to be suppressed by thermal fluctuations according to the Mermin-Wagner theorem [7], the presence of intrinsic ferromagnetism below about 45 K in single layers of CrI₃ raises the question of its driving origin(s).

The coupling between localized spins in CrI₃ is governed by different physical processes. The nature of isotropic (Heisenberg) interactions, which are usually dominant in materials with localized spins, is relatively well understood [8,9]. At the same time, the role of spin-orbit coupling is not completely elucidated. It is clearly important, as it provides a necessary source of magnetic anisotropy which breaks the spin rotational invariance, opening the gap in the magnon excitations and thus allowing for the long-range magnetic order to exist at finite temperatures [10]. However, the exact shape of the spin Hamiltonian describing bulk CrI₃ is debated. Different studies suggest the importance of Dzyaloshinskii-Moriya [11], Kitaev [12,13], or even nonrelativistic higher-order interactions [14]. As previously discussed [10], several models are equally successful in describing the inelastic neutron scattering data including the

gap of $\Delta \approx 5$ meV at the Dirac points, which points towards the existence of highly intriguing topological magnons in this material. Further experiments are needed to fully understand the nature of ferromagnetic (FM) order in CrI₃ and exploit it in applications. Magnetism in CrI₃ is also closely related to the crystal structure. At $T_S \approx 220$ K, CrI₃ features a discontinuous phase transition from the high-temperature monoclinic ($C2/m$) to the low-temperature rhombohedral ($R\bar{3}$) phase [15]. This transition is absent in few-layer systems, and different stacking patterns appear in thin and bulk samples at low temperatures, thereby affecting the evolution of magnetic order [16,17].

Here, we report high-resolution thermal expansion on bulk single crystals of CrI₃. The data show clear anomalies at the onset of bulk ferromagnetism which allow the quantitative determination of uniaxial pressure dependencies of T_C . Furthermore, we compare our experimental results with numerical calculations on the strain dependence of the dominant magnetic exchange couplings to elucidate a microscopic picture of the mechanisms governing ferromagnetism in bulk CrI₃.

Methods. The experiments were performed on CrI₃ single crystals from HQ Graphene [18] which display a structural transition at $T_S \simeq 212$ K and ferromagnetic order at $T_C = 61$ K. The magnetization was studied by means of a Physical Properties Measurement System (Quantum Design) using the vibrating sample magnetometer option. High-resolution dilatometry measurements were performed by means of a three-terminal high-resolution capacitance dilatometer in a home-built setup placed inside a variable temperature insert of an Oxford magnet system [19,20]. With this dilatometer, the relative length changes dL_i/L_i out-of-plane and in-plane, i.e., along the crystallographic c direction and in the ab plane, respectively, were studied on thin single crystals of dimensions $1.2 \times 1.8 \times 0.06$ mm³. The thermal expansion measurements were performed upon warming at a rate of 0.3 K/min. A

*yaroslav.kvashnin@physics.uu.se

†klingeler@kip.uni-heidelberg.de

point-by-point derivative of the preprocessed data yields the linear thermal expansion coefficients $\alpha_i = (1/L_i)dL_i(T)/dT$ ($i = c, \perp c$). Due to air sensitivity of the crystals, fresh samples from the same batch were utilized for the respective measurements.

For numerical studies of strain effects, the equilibrium crystal structure of bulk CrI₃ was obtained by performing a complete structural optimization within density functional theory (DFT). As for the initial guess, we adopted the parameters of the experimental low-temperature structure and kept the same point group symmetry ($R\bar{3}$) [15]. The lattice parameters and atomic positions were relaxed using the Perdew-Burke-Ernzerhof [21] functional by means of a projector augmented wave method as implemented in the VASP code [22,23]. The plane-wave kinetic energy cutoff was set to 350 eV along with a $12 \times 12 \times 12$ k -point grid. The forces on each atom were minimized down to 1 meV/Å. Once the equilibrium structure was obtained, we applied the strain within the plane of the magnetic layers (ab) as well as along the perpendicular direction (c axis). For every chosen value of strain, the positions of all the atoms in the material were optimized.

In order to extract magnetic interactions, the system was mapped onto a Heisenberg model:

$$\hat{H} = - \sum_{(i,j)} J_{ij} \mathbf{e}_i \cdot \mathbf{e}_j, \quad (1)$$

where \mathbf{e}_i is the unit vector pointing along the spin moment of a Cr³⁺ ion and J_{ij} is the exchange interaction between Cr atoms at lattice sites i and j . In this sum, we restrict ourselves to the nearest-neighbor (NN) coupling J_1 and interlayer coupling J_{\perp} . In order to calculate the exchange coupling between two selected atoms, we calculated the energies of four magnetic configurations: $|\uparrow \cdot \uparrow \cdot \uparrow \cdot \uparrow\rangle$, $|\uparrow \cdot \uparrow \cdot \uparrow \cdot \downarrow\rangle$, $|\uparrow \cdot \downarrow \cdot \uparrow \cdot \uparrow\rangle$, $|\uparrow \cdot \downarrow \cdot \downarrow \cdot \downarrow\rangle$, which we denote as $E^{\uparrow\uparrow}$, $E^{\uparrow\downarrow}$, $E^{\downarrow\uparrow}$, $E^{\downarrow\downarrow}$, respectively. The rest of the spins were pointing “up,” thus representing the FM background, corresponding to the ground state in bulk CrI₃. This way, the exchange coupling was calculated as follows:

$$J_{ij} = \frac{1}{8z} [E^{\uparrow\downarrow} + E^{\downarrow\uparrow} - (E^{\uparrow\uparrow} + E^{\downarrow\downarrow})], \quad (2)$$

where z is the number of equivalent neighbors j for a given site i . The values of J_1 and J_{\perp} were obtained for several values of in-plane and out-of-plane strain. In order to minimize the effect of more distant couplings, these calculations were performed in an orthorhombic ($\sqrt{3}a, a, c$) supercell containing 48 atoms.

There is a number of previous studies which used the same methodology to assess the magnetic exchange in CrX₃ systems both in bulk and monolayer forms [12,24–29]. The effect of strain in this class of materials was studied, for instance, in Refs. [26,30,31].

Results and discussion. The thermal expansion coefficients presented in Fig. 1(a) display anomalies in both α_c and α_{ab} at the ferromagnetic ordering temperature, thereby evidencing magnetoelastic coupling in CrI₃. While the anomaly temperatures coincide with the peak in magnetization at T_C , the anomaly in the magnetization at $T^* = 49.5$ K signaling the evolution of antiferromagnetic ordering of the surface layers [32–35] is not associated with clear anomalies in the

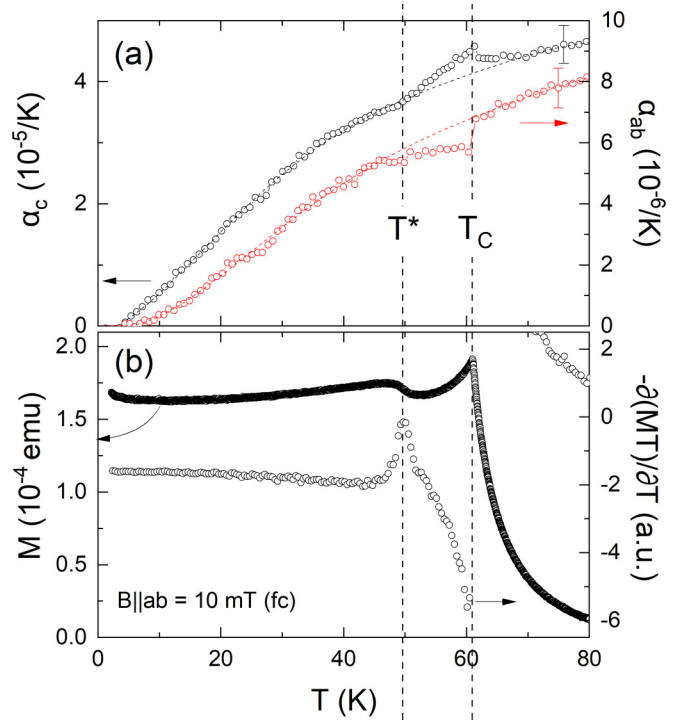


FIG. 1. (a) Thermal expansion coefficients of CrI₃, as well as (b) magnetization and its derivative, $-\partial(MT)/\partial T$, obtained at $B \parallel ab = 10$ mT in a field-cooled measurement. Dashed lines mark the ferromagnetic ordering temperature T_C and the evolution of a surface antiferromagnetic/bulk ferromagnetic phase at T^* .

thermal expansion. In addition, the out-of-plane thermal expansion also displays an anomaly at the structural transition temperature $T_S \simeq 215$ K. However, while the data are well reproducible below 150 K, this is not the case around T_S . We attribute this to irreversible stacking defects appearing in the sample at T_S and, hence, restrict the discussion to the temperature regime below 150 K [15]. In contrast, the in-plane thermal expansion data are fully reproducible and do not show any detectable anomaly in α_{ab} at T_S , i.e., there are no anomaly-related in-plane lattice changes in the detection limit $dL \approx 10^{-10}$ m (see Supplemental Material Fig. S1 [36]). Comparing in-plane and out-of-plane data, thermal expansion in CrI₃ is considerably larger along the c axis as compared to the ab plane, which is associated with very distinct directional chemical bonding. A comparably strong anisotropic behavior of the thermal expansion coefficients has been observed, for instance, in graphite, although α_{ab} becomes negative at low temperatures [37].

At $T_C = 61.5(5)$ K, the small but distinct thermal expansion anomalies in α_c and α_{ab} exhibit opposite signs, which implies opposite uniaxial pressure dependencies of T_C , i.e., $\partial T_C / \partial p_c > 0$ and $\partial T_C / \partial p_{ab} < 0$. To estimate the size of the anomalies, we fitted the thermal expansion coefficients well above T_C and well below T^* by a polynomial which is indicated in Fig. 1(a). Anomalous contributions to the thermal expansion coefficients are obtained by subtracting the polynomial background from the experimental data (see Fig. 2). Note that, by construction, this phenomenological background includes putative contributions due to magnetic

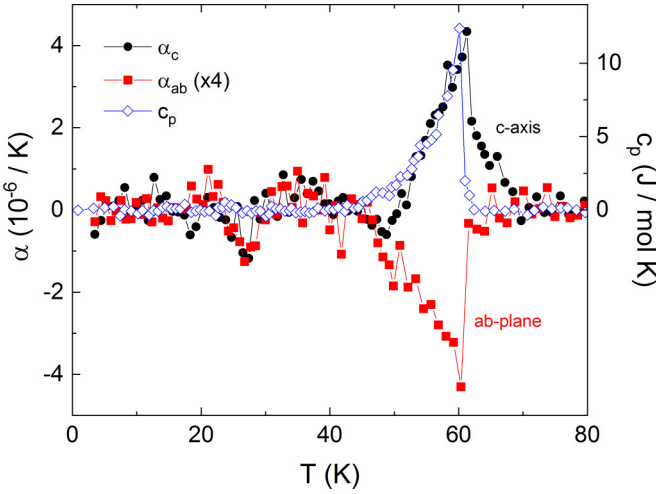


FIG. 2. Anomalous contributions to the thermal expansion coefficients and the specific heat from Ref. [38] (see the text). The data α_{ab} are multiplied by a factor 4.

short-range correlations above T_C which presence has been reported [15,38].

The anomaly at T_C is about four times larger in α_c than in α_{ab} , which implies that the corresponding in-plane and out-of-plane pressure derivatives of T_C differ by that factor, as well. Applying the same procedure for background determination to the specific heat data from Spurgeon *et al.* [38] reveals a quite similar temperature dependence of the anomalous contributions to α_i and to c_p (see Fig. 2), thereby signaling a temperature-independent Grüneisen ratio $\gamma_i = \alpha_i/c_p$, at the ferromagnetic phase transition. This experimental observation implies the presence of a single dominant energy scale ϵ^* which enables us to exploit the Grüneisen relation $V_m \gamma_i = \partial \ln \epsilon^* / \partial p_i$ [40–42]. Moreover, identifying ϵ^* with the ordering temperature T_C provides the uniaxial pressure dependencies of T_C which are listed in Table I [39,41–44].

In an alternative approach to determine $\partial T_C / \partial p_i$ from the data, we have deduced the actual jumps in the thermal expansion coefficients $\Delta \alpha_i$ and in the specific heat Δc_p at the ferromagnetic transition by means of area-conserving constructions and used the Ehrenfest relation $dT_C/dp_i = T_C V_m \Delta \alpha_i / \Delta c_p$ [45–47]. As shown in Table I, this procedure yields similar results as the above-mentioned Grüneisen analysis.

While uniaxial pressure dependencies for CrI_3 have not been reported yet, two recent studies confirm a monotonic

TABLE I. Grüneisen parameters and uniaxial pressure dependencies of $\ln \epsilon^*$ and T_C as obtained from the Grüneisen parameter (middle columns) and from the anomalies $\Delta \alpha_i$ and Δc_p (right column), for pressure applied along and perpendicularly to the c axis (see the text).

	γ_i (mol/J)	$\partial \ln \epsilon^* / \partial p_i$ (10^{-2} /GPa)	$\partial T_C / \partial p_i$ (K/GPa)	$T_C V_m \Delta \alpha_i / \Delta c_p$ (K/GPa)
$p \parallel c$	3.5×10^{-7}	2.8(5)	1.7(3)	1.5(6)
$p \perp c$	-8.7×10^{-8}	0.7(2)	-0.4(1)	-0.4(1)

increase of T_C upon the application of hydrostatic pressure [48,49]. Note that the thermodynamic analyses presented above yield the respective *initial* pressure dependencies, i.e., for $p_i \rightarrow 0$. The initial hydrostatic pressure coefficient $\partial T_C / \partial p \sim 1.3$ GPa reported by Ghosh *et al.* [48] is in good agreement with the results of our analysis in which we find $\partial T_C / \partial p = \partial T_C / \partial p_c + 2(\partial T_C / \partial p_{ab}) \approx 0.9$ K/GPa [50]. In contrast, Mondal *et al.* report a value that is roughly six times larger [49]. However, a direct comparison between the presently reported pressure dependence obtained from experimental *uniaxial* measurements with *hydrostatic* pressure experiments from the literature is not straightforwardly possible. Due to the strong structural anisotropy, the effect of hydrostatic pressure is not *a priori* clear and supposed to mainly modify the interlayer structure, such as the layer separation and stacking order, thereby effectively reflecting mainly uniaxial pressure along the c axis [51]. In general, pressure effects reported for quasi-2D honeycomb magnets in the literature vary by almost three orders of magnitude. In α - RuCl_3 , hydrostatic pressure initially suppresses long-range antiferromagnetic order at a rate of ~ 22 K/GPa [50]. Whereas, the ordering temperature in the $S = 1$ Heisenberg system $\text{Na}_3\text{Ni}_2\text{SbO}_6$ is suppressed by only ~ 0.05 K/GPa [20]. The pressure coefficient obtained from the analysis of our data on CrI_3 is in between these values and is comparable to $\partial T_N / \partial p \sim 0.7$ K/GPa found by dilatometric studies on the Kitaev iridate β - Li_2IrO_3 [47].

In the following, we compare the experimental results with *ab initio* calculations to investigate the microscopic origin of pressure evolution of magnetism in CrI_3 . The structural optimization we performed results in a NN Cr-Cr distance of 4.04 Å, which is in reasonable agreement with the experimental value of 3.96 Å [15]. The Cr-I-Cr bond angle was found to be 95° in the calculations and 93.3° in experiment. Overall, our DFT calculations result in a good description of the intralayer structural parameters. In the case of the interlayer spacing, the agreement is less good: 7.3 Å against 6.602 Å in experiment. This disagreement originates from neglecting the van der Waals interactions which govern the coupling between the layers. The estimates were shown to improve by employing vdW-corrected functionals [15]. Due to the different quality of the predicted estimates for in-plane and out-of-plane constants, one can expect the results for in-plane strain to be more reliable. However, these differences should not affect the overall trends in the changes of the exchange interactions as a function of strain.

Figure 3 shows the calculated stress for a given value of applied strain applied within the plane of the atomic layers and perpendicular to it. Here, strain is $\epsilon_i = dL_i/L_i$. It can be clearly seen that compressing the lattice along the c direction is associated with considerably smaller stress as compared to compression within the ab plane, which is an expected result for systems consisting of weakly coupled layers.

Next, we constructed supercells of the obtained crystal structures and extracted the most important exchange parameters. The results shown in Fig. 4 reveal that compressive in-plane strain tends to decrease the values of the dominant J_1 interaction while applying the stress along the c direction leads to a weak increase. Interlayer coupling J_\perp responds to both in-plane and out-of-plane compression in a similar way.

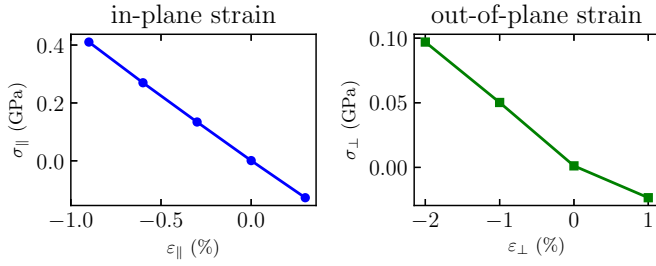


FIG. 3. Calculated stress (σ) for different values of strain (ϵ) applied along the same direction.

Being relatively small, J_{\perp} is shown to be quite sensitive to strain and is even able to change its sign from FM to anti-ferromagnetic (AFM) for a sufficiently strong compression. Similarly, numerical calculations on the strain dependence of the exchange parameters in bilayer CrI_3 also imply a transition of the magnetic interlayer coupling from AFM to FM at a compressive in-plane strain of $\sim 1\%$ [52].

Strain dependence of the exchange parameters and the T_C in monolayers of CrX_3 ($X = \text{Cl}, \text{Br}, \text{I}$) was studied in Ref. [26]. It was shown that compressive (in-plane) strain leads to the decrease of the NN Cr-Cr exchange interaction in the whole series of CrX_3 monolayers. For sufficiently large compression, the sign of the coupling even switches from ferromagnetic to antiferromagnetic. In Ref. [53] the physical origin of this change was explained in detail. In these systems, the Cr atoms are surrounded by edge-sharing octahedra and the exchange interactions are mediated by Cr-X-Cr networks. In this situation, there are two competing contributions to the NN exchange coupling [8,54–57]. First, there is a FM superexchange interaction between half-filled t_{2g} -like orbitals on one site and nominally empty e_g -like states on the neighboring Cr atom. This coupling is opposed by the AFM exchange between half-filled t_{2g} orbitals which is governed by two mechanisms: the superexchange via a single halide p orbital and *direct* kinetic exchange between the t_{2g} orbitals pointing towards each other. As one compresses the lattice, the balance between these contributions shifts and the AFM kinetic term starts to dominate, changing the sign of the total exchange integral.

Our results for the strain dependence of the NN J_1 coupling fall within the same scenario. As for J_{\perp} , this coupling is rather weak and is likely to be mediated by higher-order superexchange processes involving halide orbitals [17]. It is likely that a decrease of interlayer spacing tends to increase the overlap between wave functions involved in the dominating exchange process. In fact, this interaction is known to be strongly dependent on the layer stacking [51,58]. In our calculations we assumed the stacking not to change, which is a reasonable approximation for such small values of strain as we are dealing with here.

Summary. In summary, our high-resolution thermal expansion studies are used to elucidate and quantify magnetoelastic coupling and uniaxial pressure effects in CrI_3 . Thermal ex-

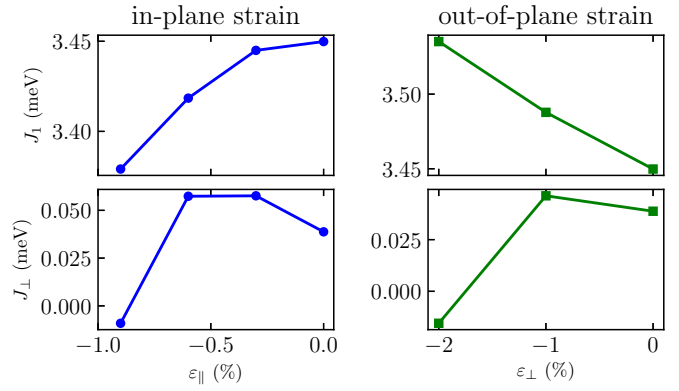


FIG. 4. Calculated nearest-neighbor (J_1) and first out-of-plane exchange interaction (J_{\perp}) as a function of strain. Positive sign of the magnetic interaction corresponds to the FM coupling.

pansion anomalies α_c and α_{ab} at the ferromagnetic ordering temperature evidence magnetoelastic coupling and imply positive (negative) pressure dependencies $\partial T_C / \partial p_i$ for pressure applied along c (ab). While uniaxial pressure applied in plane yields $\partial T_C / \partial p_{ab} \simeq -0.4 \text{ K/GPa}$, the pressure dependence on $p_{\parallel c}$ is positive and about four times larger. The response of ferromagnetism in CrI_3 to applied stress is also confirmed by numerical calculations showing that the dominating NN coupling increases as the lattice is compressed along the c direction, whereas negative in-plane strain leads to a reduction of J_1 . In contrast, interlayer exchange J_{\perp} is shown to initially increase and afterwards decrease upon the application of both out-of-plane and in-plane compression. Therefore, the experimentally observed uniaxial pressure dependencies of T_C follow that of J_1 (but not of J_{\perp}), which confirms the dominant role of J_1 for the evolution of long-range ferromagnetic order in CrI_3 . Overall, the results show that macroscopic length changes can be used to investigate microscopic parameters and in particular provide experimental values for uniaxial pressure dependencies in quasi-two-dimensional systems.

Acknowledgments. We acknowledge financial support by BMBF via the project SpinFun (13XP5088) and by Deutsche Forschungsgemeinschaft (DFG) under Germany's Excellence Strategy EXC2181/1-390900948 (the Heidelberg STRUCTURES Excellence Cluster) and through project KL 1824/13-1. Support by the Ministry of Education and Science of the Russian Federation within the framework of the governmental program of Megagrants 2020-220-08-6358 is acknowledged. We also acknowledge support by the European Union's Horizon 2020 Research and Innovation Programme, under Grant Agreement No. 824109 (European Microkelvin Platform). M.A.-H. and Y.O.K. acknowledge the financial support from the Swedish Research Council (VR) under the Projects No. 2018-05393 and No. 2019-03569, respectively. The DFT calculations were performed using the resources provided by the Swedish National Infrastructure for Computing (SNIC) at the National Supercomputing Centre (NSC).

- [1] B. Huang, G. Clark, E. Navarro-Moratalla, D. R. Klein, R. Cheng, K. L. Seyler, D. Zhong, E. Schmidgall, M. A. McGuire, D. H. Cobden *et al.*, *Nature (London)* **546**, 270 (2017).
- [2] C. Gong, L. Li, Z. Li, H. Ji, A. Stern, Y. Xia, T. Cao, W. Bao, C. Wang, Y. Wang *et al.*, *Nature (London)* **546**, 265 (2017).
- [3] D. J. O'Hara, T. Zhu, A. H. Trout, A. S. Ahmed, Y. K. Luo, C. H. Lee, M. R. Brenner, S. Rajan, J. A. Gupta, D. W. McComb *et al.*, *Nano Lett.* **18**, 3125 (2018).
- [4] X. Sun, W. Li, X. Wang, Q. Sui, T. Zhang, Z. Wang, L. Liu, D. Li, S. Feng, S. Zhong *et al.*, *Nano Res.* **13**, 3358 (2020).
- [5] R. B. Jenjeti, R. Kumar, M. P. Austeria, and S. Sampath, *Sci. Rep.* **8**, 8586 (2018).
- [6] H. Idzuchi, A. E. Llacsahuanga Allcca, X. C. Pan, K. Tanigaki, and Y. P. Chen, *Appl. Phys. Lett.* **115**, 232403 (2019).
- [7] N. D. Mervin and H. Wagner, *Phys. Rev. Lett.* **17**, 1133 (1966).
- [8] O. Besbes, S. Nikolaev, N. Meskini, and I. Solovyev, *Phys. Rev. B* **99**, 104432 (2019).
- [9] D. Soriano, M. I. Katsnelson, and J. Fernández-Rossier, *Nano Lett.* **20**, 6225 (2020).
- [10] L. Chen, J. H. Chung, T. Chen, C. Duan, A. Schneidewind, I. Radelytskyi, D. J. Voneshen, R. A. Ewings, M. B. Stone, A. I. Kolesnikov, B. Winn, S. Chi, R. A. Mole, D. H. Yu, B. Gao, and P. Dai, *Phys. Rev. B* **101**, 134418 (2020).
- [11] L. Chen, J.-H. Chung, B. Gao, T. Chen, M. B. Stone, A. I. Kolesnikov, Q. Huang, and P. Dai, *Phys. Rev. X* **8**, 041028 (2018).
- [12] C. Xu, J. Feng, H. Xiang, and L. Bellaïche, *npj Comput. Mater.* **4**, 57 (2018).
- [13] I. Lee, F. G. Utermohlen, D. Weber, K. Hwang, C. Zhang, J. van Tol, J. E. Goldberger, N. Trivedi, and P. C. Hammel, *Phys. Rev. Lett.* **124**, 017201 (2020).
- [14] A. Kartsev, M. Augustin, R. F. L. Evans, K. S. Novoselov, and E. J. G. Santos, *npj Comput. Mater.* **6**, 150 (2020).
- [15] M. A. McGuire, H. Dixit, V. R. Cooper, and B. C. Sales, *Chem. Mater.* **27**, 612 (2015).
- [16] N. Ubrig, Z. Wang, J. Teyssier, T. Taniguchi, K. Watanabe, E. Giannini, A. F. Morpurgo, and M. Gilbertini, *2D Mater.* **7**, 015007 (2020).
- [17] N. Sivadas, S. Okamoto, X. Xu, C. J. Fennie, and D. Xiao, *Nano Lett.* **18**, 7658 (2018).
- [18] www.hqgraphene.com.
- [19] R. Küchler, T. Bauer, M. Brando, and F. Steglich, *Rev. Sci. Instrum.* **83**, 095102 (2012).
- [20] J. Werner, W. Hergett, M. Gertig, J. Park, C. Koo, and R. Klingeler, *Phys. Rev. B* **95**, 214414 (2017).
- [21] J. P. Perdew, K. Burke, and M. Ernzerhof, *Phys. Rev. Lett.* **77**, 3865 (1996).
- [22] G. Kresse and D. Joubert, *Phys. Rev. B* **59**, 1758 (1999).
- [23] G. Kresse and J. Furthmüller, *Comput. Mater. Sci.* **6**, 15 (1996).
- [24] X. Lu, R. Fei, and L. Yang, *Phys. Rev. B* **100**, 205409 (2019).
- [25] J. L. Lado and F. Fernández-Rossier, *2D Mater.* **4**, 035002 (2017).
- [26] L. Webster and J. A. Yan, *Phys. Rev. B* **98**, 144411 (2018).
- [27] C. Xu, J. Feng, S. Prokhorenko, Y. Nahas, H. Xiang, and L. Bellaïche, *Phys. Rev. B* **101**, 060404(R) (2020).
- [28] T. Olsen, *MRS Commun.* **9**, 1142 (2019).
- [29] F. Xue, Y. Hou, Z. Wang, and R. Wu, *Phys. Rev. B* **100**, 224429 (2019).
- [30] W. Zhang, Q. Qu, P. Zhu, and C. Lam, *J. Mater. Chem. C* **3**, 12457 (2015).
- [31] M. Pizzochero and O. V. Yazyev, *J. Phys. Chem. C* **124**, 7585 (2020).
- [32] B. Niu, T. Su, B. A. Francisco, S. Ghosh, F. Kargar, X. Huang, M. Lohmann, J. Li, Y. Xu, T. Taniguchi *et al.*, *Nano Lett.* **20**, 553 (2020).
- [33] S. Li, Z. Ye, X. Luo, G. Ye, H. H. Kim, B. Yang, S. Tian, C. Li, H. Lei, A. W. Tsen, K. Sun, R. He, and L. Zhao, *Phys. Rev. X* **10**, 011075 (2020).
- [34] A. McCreary, T. T. Mai, F. G. Utermohlen, J. R. Simpson, K. F. Garrity, X. Feng, D. Shcherbakov, Y. Zhu, J. Hu, D. Weber *et al.*, *Nat. Commun.* **11**, 3879 (2020).
- [35] Y. Liu, L. Wu, X. Tong, J. Li, J. Tao, and C. Petrovic, *Sci. Rep.* **9**, 13599 (2019).
- [36] See Supplemental Material at <http://link.aps.org/supplemental/10.1103/PhysRevB.105.L060404> for the in-plane length changes in CrI₃ from 2K to 250 K.
- [37] J. E. Zorzi and C. Perottoni, *Comput. Mater. Sci.* **199**, 110719 (2021).
- [38] K. Spurgeon, G. Kozłowski, M. A. Susner, Z. Turgut, and J. Boeckl, *SCIREA J. Elec. Eng.* **5**, 141 (2020).
- [39] Error bars in the table stem from the macroscopic sample length, background determination, and scaling.
- [40] T. Lorenz, S. Stark, O. Heyer, N. Hollmann, A. Vasiliev, A. Oosawa, and H. Tanaka, *J. Magn. Magn. Mater.* **316**, 291 (2007).
- [41] O. Heyer, P. Link, D. Wandner, U. Ruschewitz, and T. Lorenz, *New J. Phys.* **13**, 113041 (2011).
- [42] R. Klingeler, J. Geck, S. Arumugam, N. Tristan, P. Reutler, B. Büchner, L. Pinsard-Gaudart, and A. Revcolevschi, *Phys. Rev. B* **73**, 214432 (2006).
- [43] P. Gegenwart, *Rep. Prog. Phys.* **79**, 114502 (2016).
- [44] M. Hoffmann, K. Dey, J. Werner, R. Bag, J. Kaiser, H. Wadepohl, Y. Skourski, M. Abdel-Hafiez, S. Singh, and R. Klingeler, *Phys. Rev. B* **104**, 014429 (2021).
- [45] R. Küchler, Ph.D. thesis, Technische Universität Dresden, 2005.
- [46] C. Meingast, B. Blank, H. Bürkle, B. Obst, T. Wolf, H. Wühl, V. Selvamanickam, and K. Salama, *Phys. Rev. B* **41**, 11299 (1990).
- [47] M. Majumder, R. S. Manna, G. Simutis, J. C. Orain, T. Dey, F. Freund, A. Jesche, R. Khasanov, P. K. Biswas, E. Bykova, N. Dubrovinskaia, L. S. Dubrovinsky, R. Yadav, L. Hozoi, S. Nishimoto, A. A. Tsirlin, and P. Gegenwart, *Phys. Rev. Lett.* **120**, 237202 (2018).
- [48] A. Ghosh, D. Singh, Q. Mu, Y. Kvashnin, G. Haider, M. Jonak, D. Chareev, T. Aramaki, S. A. Medvedev, R. Klingeler *et al.*, *Phys. Rev. B* **105**, L081104 (2022).
- [49] S. Mondal, M. Kannan, M. Das, L. Govindaraj, R. Singha, B. Satpati, S. Arumugam, and P. Mandal, *Phys. Rev. B* **99**, 180407(R) (2019).
- [50] M. He, X. Wang, L. Wang, F. Hardy, T. Wolf, P. Adelman, T. Brückel, Y. Su, and C. Meingast, *J. Phys.: Condens. Matter* **30**, 385702 (2018).
- [51] T. Li, S. Jiang, N. Sivadas, Z. Wang, Y. Xu, D. Weber, J. Goldberger, K. Watanabe, T. Taniguchi, C. J. Fennie *et al.*, *Nat. Mater.* **18**, 1303 (2019).
- [52] A. M. León, J. W. González, J. Mejía-López, F. C. de Lima, and E. S. Morell, *2D Mater.* **7**, 035008 (2020).

- [53] M. Dupont, Y. O. Kvashnin, M. Shiranzaei, J. Fransson, N. Laflorencie, and A. Kantian, *Phys. Rev. Lett.* **127**, 037204 (2021).
- [54] P. W. Anderson, *Phys. Rev.* **115**, 2 (1959).
- [55] J. Kanamori, *J. Phys. Chem. Solids* **10**, 87 (1959).
- [56] J. B. Goodenough, *J. Phys. Chem. Solids* **6**, 287 (1958).
- [57] I. V. Kashin, V. V. Mazurenko, M. I. Katsnelson, and A. N. Rudenko, *2D Mater.* **7**, 025036 (2020).
- [58] T. Song, Z. Fei, M. Yankowitz, Z. Lin, Q. Jiang, K. Hwangbo, Q. Zhang, B. Sun, T. Taniguchi, K. Watanabe *et al.*, *Nat. Mater.* **18**, 1298 (2019).